Stark Many-Body Localization Induced Quantum Mpemba Effect

Yi-Rui Zhang , Han-Ze Li , Xuyang Huang , Yu-Jun Zhao , Jian-Xin Zhong *

Posted Date: 15 February 2026

doi: 10.20944/preprints202602.1143.v1

Keywords: stark many-body localization; quantum mpemba effect; entanglement asymmetry; symme-try restoration; non-equilibrium dynamics

Article

Stark Many-Body Localization Induced Quantum Mpemba Effect

Yi-Rui Zhang [1,†], Han-Ze Li [1,2,†], Xuyang Huang [1], Yu-Jun Zhao [1,3] and Jian-Xin Zhong [1,3,*]

[1] Institute for Quantum Science and Technology, Shanghai University, Shanghai 200444, China
[2] Department of Physics, National University of Singapore, Singapore 117542, Singapore
[3] School of Physics and Optoelectronics, Xiangtan University, Xiangtan 411105, China
[†] These two authors contributed equally to this work.
[*] Correspondence: jxzhong@shu.edu.cn

Abstract

The quantum Mpemba effect (QME) describes the counterintuitive phenomenon where a system initially further from equilibrium relaxes faster than one closer to it. Specifically, the QME associated with symmetry restoration has been extensively investigated across integrable, ergodic, and disordered localized systems. However, its fate in disorder-free ergodicity-breaking settings, such as the Stark many-body localized (Stark-MBL) phase, remains an open question. Here, we explore the dynamics of local $U(1)$ symmetry restoration in a Stark-MBL XXZ spin-$\frac{1}{2}$ chain, using the Rényi-2 entanglement asymmetry (EA) as a probe. Using an analytical operator-string expansion supported by numerical simulations, we demonstrate that the QME transitions from an initial-state-dependent anomaly in the ergodic phase to a universal feature in the Stark-MBL regime. Moreover, the Mpemba time scales exponentially with the subsystem size even in the absence of global transport, governed by high-order off-resonant processes. We attribute this robust inversion to a Stark-induced hierarchy of relaxation channels that fundamentally constrains the effective Hilbert space dimension. The findings pave the way for utilizing tunable potentials to engineer and control anomalous relaxation timescales in quantum technologies without reliance on quenched disorder.

Keywords: stark many-body localization; quantum mpemba effect; entanglement asymmetry; symmetry restoration; non-equilibrium dynamics

1. Introduction

Understanding how isolated quantum many-body systems lose locally accessible information about their initial conditions is a central problem in non-equilibrium physics [1,1,2]. In generic interacting settings, the eigenstate thermalization hypothesis [3,4] suggests that after a global quench small subsystems approach stationary reduced states determined by conservation laws. When a global $U(1)$ charge Q is conserved, this relaxation has a particularly transparent structural signature: the reduced density matrix of a subregion, $\rho_A(t)$, progressively becomes compatible with the charge-sector decomposition set by the restricted charge Q_A, so that coherences between different Q_A sectors are suppressed and local properties become consistent with an equilibrium description constrained by energy and charge [5,6].

This structural relaxation is commonly referred to as symmetry restoration [7–15] at the subsystem level. To diagnose this, the EA [16] is utilized: a symmetry-sensitive quantity constructed from $\rho_A(t)$ that measures the remaining locally accessible symmetry-breaking information and vanishes when $\rho_A(t)$ becomes symmetric with respect to Q_A. Because it is defined solely from the reduced state and directly targets inter-sector coherence, EA provides a experimental and theoretical proof of symmetry restoration in unitary dynamics. Symmetry restoration also exposes a counterintuitive ordering phenomenon. The QME (see recent reviews [17,18]) captures the possibility that, under identical dynamics, an initial state that is farther from the stationary structure can relax faster than

 doi:10.20944/preprints202602.1143.v1

one that starts closer. Quantum Mpemba behaviour has been explored in both open [19–47] and closed [16,48–70] systems. Here, unless stated otherwise, we use the term, QME, exclusively in the closed-system sense, where the effect is diagnosed through local equilibration under unitary time evolution. Recent works [16,48–70] have shown that this closed-system Mpemba phenomenology arises in Hamiltonian many-body dynamics and in symmetric random quantum circuits, where conservation laws are enforced at the level of local gates and the dynamics provides a minimal setting for unitary thermalization. In the symmetry-restoration context, the Mpemba effect corresponds to an inversion of restoration times, meaning that a more strongly symmetry-broken initial condition can restore symmetry faster according to symmetry-resolved diagnostics such as EA.

Thus, the key motivation of this work is to understand whether such symmetry-restoration Mpemba inversions persist when ergodicity is impeded. Localization [71] provides a natural route to non-ergodic unitary dynamics and long-lived memory, and it reshapes relaxation by restricting which parts of Hilbert space are dynamically explored on accessible time scales. This makes symmetry restoration strongly preparation dependent and suggests a natural mechanism for inversions [62]: different initial states can expand the effectively explored, symmetry-allowed Hilbert space at different rates, leading to different rates of sector redistribution and intra-sector mixing in $\rho_A(t)$, and hence to different decay rates of EA.

Many-body localization has already provided evidence that Mpemba-type inversions can occur even in non-ergodic dynamics [62]. This raises an immediate and practically important question: is the phenomenon tied to quenched randomness, or does it survive in non-ergodic settings driven by a different microscopic mechanism? Stark-MBL [72–74] offers a complementary route to localization that is induced by a uniform potential gradient rather than disorder. It avoids sample-to-sample fluctuations, reduces the reliance on disorder averaging, and introduces a continuously tunable control parameter, the field strength, that allows one to traverse ergodic and non-ergodic regimes within a single Hamiltonian family. These features make Stark-MBL an ideal platform to interrogate symmetry restoration and its Mpemba inversion in a controlled manner, and to connect the inversion directly to how a potential gradient reorganizes resonant processes and constrains the growth of the dynamically explored Hilbert space.

In this work, we have provided a comprehensive analysis of symmetry restoration and the QME within the context of Stark-MBL. By investigating the dynamics of the Rényi-2 EA in a tilted XXZ chain, we revealed that the Stark-induced breaking of ergodicity leads to a robust and universal Mpemba effect. Our central findings regarding the phase dependence of the QME are summarized below (see table in Fig. 1):

- In the *ergodic phase*, the occurrence of the QME is contingent upon the microscopic details of the initial state. Specifically, it is present for the Tilted Ferromagnetic State (TFS) but absent for the Tilted Néel State (TNS), as the relaxation is governed by the dimension of the dynamically accessible charge sectors.
- In the *Stark-MBL phase*, the QME becomes a universal phenomenon. It emerges for both TNS and TFS initial states. This universality arises from a Stark-induced inversion of the steady-state ordering, where stronger initial symmetry breaking leads to a more symmetric local steady state due to the restricted effective Hilbert space dimension.

Furthermore, we analytically determined the characteristic timescale of this anomalous relaxation. We found that the Mpemba time t_M is governed by high-order perturbative processes and scales exponentially with the subsystem size, $t_M \propto (F/J)^{N_A-1}$. This prediction is quantitatively corroborated by exact diagonalization simulations, confirming that symmetry restoration in the Stark-MBL phase is driven by slow, off-resonant quantum fluctuations rather than diffusive transport.

These results place Mpemba-type anomalies into a tunable localization setting without quenched disorder, offering a clear protocol to observe this effect in state-of-the-art quantum simulators such as trapped ions or superconducting circuits. Broadly, our work paves the way for utilizing tunable

 doi:10.20944/preprints202602.1143.v1

potentials to engineer anomalous relaxation timescales, providing new insights into the interplay between ergodicity breaking and symmetry-protected quantum information.

Regimes \ Initial states	TNS	TFS
Ergodic $(F < F_c)$	No QME	With QME
Stark MBL $(F > F_c)$	Emergent QME	With QME

Figure 1. Comparison of the presence of QME in the ergodic region (first row) and the Stark-MBL region (second row) for the different initial states (TFS and TNS) considered in this work.

2. Methods

2.1. Model Hamiltonian

We study a one-dimensional spin-1/2 XXZ chain in the presence of a linear Stark potential. The Hamiltonian is given by:

$$H = -J \sum_{i=1}^{N-1} \left(S_i^x S_{i+1}^x + S_i^y S_{i+1}^y \right) + \Delta \sum_{i=1}^{N-1} S_i^z S_{i+1}^z + \sum_{i=1}^{N} [Fi + (i/N)^2] S_i^z, \tag{1}$$

where S_i^α ($\alpha \in \{x, y, z\}$) are the spin-1/2 operators at site i, satisfying the commutation relations $[S_i^\alpha, S_j^\beta] = i\delta_{ij}\epsilon_{\alpha\beta\gamma}S_i^\gamma$. Here, J sets the energy scale of the hopping set to $J = 2$ hereafter, Δ represents the nearest-neighbor interaction anisotropy, and F denotes the strength of the effective electric field the Stark potential gradient. We employ open boundary conditions to accommodate the linear potential. The quadratic term $(i/N)^2$ is included as a smooth boundary regularization to gently lift finite-size near-degeneracies of the perfectly linear tilt and suppress long-lived coherent oscillations, thereby stabilizing the late-time dephasing behavior [72].

The model conserves the total magnetization $Q = \sum_i S_i^z$, exhibiting a global $U(1)$ symmetry. The interplay between the interaction Δ and the tilt F governs the transition from an ergodic thermalizing phase to a Stark-MBL phase, where transport is suppressed, and the system breaks ergodicity.

2.2. Rényi-2 Entanglement Asymmetry

To quantify the restoration of the $U(1)$ symmetry within a local subsystem, we utilize the EA. We partition the system into a subsystem A of size N_A and its complement B. The state of the subsystem is described by the reduced density matrix $\rho_A(t) = \mathrm{Tr}_B[|\psi(t)\rangle\langle\psi(t)|]$. The global $U(1)$ symmetry implies the existence of a local charge operator $Q_A = \sum_{i\in A} S_i^z$. If the symmetry is locally broken, $[\rho_A(t), Q_A] \neq 0$. The symmetrized state, which retains only the diagonal blocks in the charge basis, is obtained via the twirling map:

$$\rho_{A,Q}(t) = \sum_q \Pi_q \rho_A(t) \Pi_q = \frac{1}{2\pi} \int_0^{2\pi} d\phi \, e^{-i\phi Q_A} \rho_A(t) e^{i\phi Q_A}, \tag{2}$$

where Π_q is the projector onto the eigenspace of Q_A with charge q. The EA is defined as the difference between the entanglement entropy of the symmetrized state and the original state. We specifically employ the Rényi-2 EA, $\Delta S_A^{(2)}$, due to its analytical tractability:

$$\Delta S_A^{(2)}(t) = S^{(2)}(\rho_{A,Q}(t)) - S^{(2)}(\rho_A(t)), \tag{3}$$

 doi:10.20944/preprints202602.1143.v1

where the Rényi-2 entropy is $S^{(2)}(\rho) = -\log \mathrm{Tr}(\rho^2)$. Substituting this definition, the asymmetry can be expressed as the logarithm of the ratio of purities:

$$\Delta S_A^{(2)}(t) = \log\left(\frac{\mathrm{Tr}(\rho_A^2(t))}{\mathrm{Tr}(\rho_{A,Q}^2(t))}\right). \tag{4}$$

This quantity is strictly non-negative, $\Delta S_A^{(2)}(t) \geq 0$, and vanishes if and only if the state is $U(1)$ symmetric, i.e., $[\rho_A, Q_A] = 0$.

2.3. Operator Space Expansion

To analyze the dynamical mechanism of symmetry restoration, it is convenient to expand the density matrix in an orthonormal operator basis. The set of operator strings $P = \prod_{i\in A} \mathcal{O}_i$, where $\mathcal{O}_i \in \{I_i, S_i^+, S_i^-, S_i^z\}$, forms a complete basis for operators on subsystem A with $S_i^{\pm} = \frac{1}{\sqrt{2}}(S_i^x \pm iS_i^y)$. We normalize the basis such that $\mathrm{Tr}(P^\dagger P') = 2^{N_A}\delta_{P,P'}$. The purity of the reduced density matrix can then be expanded as:

$$\mathrm{Tr}(\rho_A^2(t)) = \frac{1}{2^{N_A}} \sum_{P\subset A} |\langle\psi(t)|P|\psi(t)\rangle|^2 \equiv \frac{1}{2^{N_A}} f(t), \tag{5}$$

where $f(t)$ represents the total weight of all operator strings.

Similarly, the purity of the symmetrized state $\rho_{A,Q}$ contains contributions only from charge-conserving strings, those satisfying $[P, Q_A] = 0$:

$$\mathrm{Tr}(\rho_{A,Q}^2(t)) = \frac{1}{2^{N_A}} \sum_{P\subset A:[P,Q_A]=0} |\langle\psi(t)|P|\psi(t)\rangle|^2 \equiv \frac{1}{2^{N_A}} f^c(t). \tag{6}$$

Substituting these into Eq. (4), the Rényi-2 EA, then, becomes:

$$\Delta S_A^{(2)}(t) = \log\left(\frac{f(t)}{f^c(t)}\right). \tag{7}$$

Here, $f(t)$ sums over all strings, while $f^c(t)$ sums only over the diagonal strings that preserve the local charge.

The dynamics of $\Delta S_A^{(2)}(t)$, Eq. (7), are thus governed by the relative decay rates of charge-neutral versus charge-non-conserving operator strings.

2.4. Quantum Mpemba Effect

The QME describes an anomalous relaxation phenomenon where a system initially further from equilibrium relaxes faster than one initially closer. We consider a family of initial states parametrized by a tilt angle θ, denoted as $|\psi_\theta\rangle$. The distance from symmetry at time t is quantified by $\Delta S_A^{(2)}(t;\theta)$. We assume that the initial asymmetry $\Delta S_A^{(2)}(0;\theta)$ is monotonically increasing with $\theta \in (0, \frac{\pi}{2}]$, i.e., "hotter" states have larger initial asymmetry.

A QME is defined to occur iff there exist two parameters $\theta_h > \theta_c$ such that:

$$\Delta S_A^{(2)}(0;\theta_h) > \Delta S_A^{(2)}(0;\theta_c), \tag{8}$$

but at some later time $t > t_M$ (the Mpemba time):

$$\Delta S_A^{(2)}(t;\theta_h) < \Delta S_A^{(2)}(t;\theta_c). \tag{9}$$

Specifically, we investigate the existence of this in the Stark-MBL regime, where non-ergodicity may protect certain operator sectors, leading to non-trivial relaxation hierarchies.

 doi:10.20944/preprints202602.1143.v1

3. Results

3.1. Analytical Results

3.1.1. From the Stark Hamiltonian to an Effective Diagonal Description

We start from Eq. (1) and focus on the strong-tilt regime $F \gg J, \Delta$. We decompose $H = H_0 + V$ with

$$H_0 = \sum_{i=1}^{N} \left[Fi + (i/N)^2 \right] S_i^z + \Delta \sum_{i=1}^{N-1} S_i^z S_{i+1}^z, \tag{10}$$

$$V = -J \sum_{i=1}^{N-1} \left(S_i^x S_{i+1}^x + S_i^y S_{i+1}^y \right) = -\frac{J}{2} \sum_{i=1}^{N-1} \left(S_i^+ S_{i+1}^- + S_i^- S_{i+1}^+ \right). \tag{11}$$

In the Dirac picture with respect to H_0, each nearest-neighbor flip-flop term acquires a rapidly oscillating phase $e^{\pm i[(\varepsilon_{i+1} - \varepsilon_i) + \Delta \delta_i]t}$, where $\varepsilon_i = Fi + (i/N)^2$ and δ_i is an $O(1)$ operator-valued shift set by the adjacent S^z configuration. Since $\varepsilon_{i+1} - \varepsilon_i \simeq F$ dominates for $F \gg J, \Delta$, these terms are strongly off-resonant and average out on the long-time scales relevant for the late-time envelopes discussed below.

Consequently, to leading order in J/F, the dynamics is governed by an effective Hamiltonian obtained by perturbatively eliminating V (equivalently via a Schrieffer–Wolff transformation). In the strong-Stark limit this effective Hamiltonian is (quasi-)diagonal in the computational basis and takes the generic form

$$H_{\text{eff}} = \sum_i h_i S_i^z + \sum_{i<j} J_{ij} S_i^z S_j^z + \cdots, \tag{12}$$

where $h_i \approx Fi + (i/N)^2$ up to $O(J^2/F)$ corrections, and the longitudinal couplings J_{ij} arise from virtual sequences of the flip-flop processes and decay rapidly with distance. For our purposes the crucial point is that H_{eff} generates configuration-dependent phases in the S^z basis, which dephase expectation values of operator strings containing $S^\pm$ at late times.

3.1.2. Stark Many-Body Localized EA Plateau

We now derive the late-time plateau rules for the operator-string weights entering the Rényi-2 EA (7). We consider the same tilted product initial-state families as in the main text, namely the TFS and the TNS. Let $\{|0\rangle, |1\rangle\}$ denote the local eigenstates of computational basis S_i^z. The TFS is the uniform tilted product state

$$|\psi_\theta^{\text{TFS}}\rangle = \left(\cos(\tfrac{\theta}{2}) |0\rangle + \sin(\tfrac{\theta}{2}) |1\rangle \right)^{\otimes N}. \tag{13}$$

The TNS differs only by a staggered relative phase between the $|0\rangle$ and $|1\rangle$ components,

$$|\psi_\theta^{\text{TNS}}\rangle = \bigotimes_{i=1}^{N} \left(\cos(\tfrac{\theta}{2}) |0\rangle + (-1)^i \sin(\tfrac{\theta}{2}) |1\rangle \right). \tag{14}$$

In both cases the computational-basis probabilities are identical and site independent, $|\langle \sigma | \psi_\theta \rangle|^2 = \prod_{i=1}^{N} p_{\sigma_i}$ with $p_0 = \cos^2(\theta/2)$ and $p_1 = \sin^2(\theta/2)$.

In the effective diagonal dynamics of Sec. 3.1.1, operator strings containing at least one $S^\pm$ acquire rapidly varying configuration-dependent phases. After long-time averaging, off-diagonal contributions dephase and one obtains a diagonal-probability expression whose magnitude factorizes into single-site contributions. Each site on which P contains $S^\pm$ enforces a flip between the paired computational configurations and contributes a factor $2p_0p_1$, whereas each site with I or S^z contributes $p_0^2 + p_1^2$. It is therefore convenient to define

$$a_\theta \equiv p_0^2 + p_1^2 = \cos^4(\theta/2) + \sin^4(\theta/2) = \frac{1 + \cos^2\theta}{2}, \tag{15}$$

$$b_\theta \equiv 2p_0p_1 = 2\cos^2(\theta/2)\sin^2(\theta/2) = \frac{\sin^2\theta}{2}. \tag{16}$$

 doi:10.20944/preprints202602.1143.v1

Then for any operator string with $n_{\mathrm{chg}}(P) = \#(S^+) + \#(S^-) \geq 1$, the late-time plateau obeys

$$\overline{|\langle\psi(t)|P|\psi(t)\rangle|^2} \simeq b_\theta^{\,n_{\mathrm{chg}}(P)}\, a_\theta^{\,N-n_{\mathrm{chg}}(P)}. \tag{17}$$

The factor $a_\theta^{N-n_{\mathrm{chg}}(P)}$ includes contributions from sites outside A because the long-time dephasing expression involves full-system probabilities $|\langle\sigma|\psi_\theta\rangle|^4$. For purely diagonal strings $P \in \{I, S^z\}^{\otimes N_A}$ one has $[P, H_{\mathrm{eff}}] = 0$, so their expectation values are time independent. Summing their squared expectations in the above operator normalization gives the exact identity

$$\sum_{P\in\{I,S^z\}^{\otimes N_A}} |\langle\psi(t)|P|\psi(t)\rangle|^2 = (1+\cos^2\theta)^{N_A} = 2^{N_A} a_\theta^{N_A}. \tag{18}$$

We now compute the long-time limits of $f(t)$ and $f^c(t)$ defined in Sec. 2. A convenient way to obtain $f(\theta,\infty) = \sum_{P\subset A} \overline{|\langle P(t)\rangle|^2}$ is: (i) apply the plateau rule Eq. (17) to all 4^{N_A} strings, and (ii) replace the purely diagonal subset $P \in \{I, S^z\}^{\otimes N_A}$ by its exact contribution Eq. (18).

Step (i): summing Eq. (17) over all strings amounts to summing, on each site in A, the four local contributions I, S^z, S^+, S^-, which yields

$$(a_\theta + a_\theta + b_\theta + b_\theta) = 2(a_\theta + b_\theta) = 2, \tag{19}$$

since $a_\theta + b_\theta = (p_0 + p_1)^2 = 1$. Thus the plateau sum over all strings is $2^{N_A} a_\theta^{N-N_A}$.

Step (ii): within that plateau sum, the diagonal subset contributes $2^{N_A} a_\theta^{N}$, while its exact value is $2^{N_A} a_\theta^{N_A}$. Replacing the diagonal subset therefore gives

$$f(\theta,\infty) = 2^{N_A}\left(a_\theta^{N_A} + a_\theta^{N-N_A} - a_\theta^{N}\right). \tag{20}$$

For $f^c(\theta,\infty)$, by definition only charge-neutral strings with $[P, Q_A] = 0$ contribute. All diagonal strings are charge-neutral, hence $f^c(\theta,\infty) \geq 2^{N_A} a_\theta^{N_A}$. Additional charge-neutral contributions arise from strings containing equal numbers of S^+ and S^- within A. These form a strict subset of the spin-changing strings and their total contribution is bounded by the total spin-changing weight, giving

$$0 \leq f^c(\theta,\infty) - 2^{N_A} a_\theta^{N_A} \leq 2^{N_A}\left(a_\theta^{N-N_A} - a_\theta^{N}\right). \tag{21}$$

In finite N with $\theta \in (0, \frac{\pi}{2}]$, so that $a_\theta < 1$ and $N_A/N < 1/2$, this correction is parametrically small compared with $2^{N_A} a_\theta^{N_A}$. To leading order we therefore take

$$f^c(\theta,\infty) \simeq 2^{N_A} a_\theta^{N_A}. \tag{22}$$

Thus, the steady-state plateau prediction $\Delta S_A^{(2)}(\infty) = \log \frac{f(\theta,\infty)}{f^c(\theta,\infty)} \simeq \log\left[1 + a_\theta^{N-2N_A} - a_\theta^{N-N_A}\right]$. When $a_\theta^{N-2N_A} \ll 1$, we obtain

$$\Delta S_A^{(2)}(\infty) \simeq a_\theta^{N-2N_A}\left(1 - a_\theta^{N_A}\right). \tag{23}$$

Note that the above plateau rule depends on the initial state only through the computational-basis probabilities $|\langle\sigma|\psi_\theta\rangle|^2$. Since TFS and TNS differ only by site-dependent phases, they share the same $|\langle\sigma|\psi_\theta\rangle|^2$ and hence yield identical plateau predictions for $f(\infty)$, $f^c(\infty)$, and $\Delta S_A^{(2)}(\infty)$.

3.1.3. Emergent QME in Stark Many-Body Localization and Mpemba-Time Scaling

We now elucidate the physical mechanism underlying the emergent QME and its Rényi-2 EA QME time scaling properties.

First, we address the question of symmetry restoration. In the Stark-MBL regime, the system is non-ergodic and does not relax to a thermal Gibbs ensemble. However, this does not imply that

 doi:10.20944/preprints202602.1143.v1

local subsystems retain all information about the initial symmetry breaking. As shown by Eqs. (20) and (22), in the thermodynamic limit $N \to \infty$ with fixed subsystem size N_A, the steady-state EA is controlled by the term $a_\theta^{N-2N_A}$. Since $a_\theta < 1$ for any $\theta > 0$, this term vanishes as $N \to \infty$. Consequently, $\Delta S_A^{(2)}(\infty) \to 0$. This indicates that even in the absence of global transport, the dephasing induced by the Stark potential is sufficient to destroy off-diagonal coherences between charge sectors locally, thereby restoring the $U(1)$ symmetry at the subsystem level.

Second, we determine the existence of the QME and its physical origin. The Stark-MBL regime is governed by a fundamentally different mechanism than the ergodic regime, leading to distinct behaviors for the TNS [also see Fig. 1]:

- *Ergodic Regime:* Symmetry restoration is governed by the dimension of the dynamically accessible Hilbert space sectors.
  - For the *TNS*, the untilted state ($\theta = 0$) resides in the half-filling sector ($Q = 0$), which has the maximal Hilbert space dimension and thus the fastest thermalization rate. Increasing the tilt θ spreads the wavefunction into charge sectors away from half-filling, which have smaller dimensions and slower relaxation rates. Since the state with larger initial asymmetry relaxes slower, the EA curves do not cross, and *QME is absent for the TNS*.
  - For the *TFS*, the situation is reversed. The un-tilted state resides at the edge of the spectrum. Increasing θ moves the state toward the central, high-dimension sectors, accelerating relaxation. Thus, *QME is present*.
- *Stark-MBL Regime:* Relaxation is governed by dephasing in the effective diagonal basis, and the existence of QME is determined by the ordering of the steady-state values.
  - As derived in Eq. (23), the steady-state plateau $\Delta S_A^{(2)}(\infty)$ scales with $a_\theta^{N-2N_A}$. Since $a_\theta = (1 + \cos^2\theta)/2$ is a monotonically decreasing function of θ, a larger initial tilt θ (higher initial asymmetry) leads to a lower steady-state asymmetry.
  - This *inversion of ordering*, high initial value leading to low final value, mathematically guarantees that the EA evolution curves for different θ must cross at intermediate times. Consequently, *QME becomes universal in the Stark-MBL regime*, appearing for both TNS and TFS regardless of their ergodic behavior.

Finally, we estimate the scaling of the Mpemba time t_M. In the strong Stark limit ($F \gg J$), restoring symmetry within a subsystem of size N_A requires quantum fluctuations that couple different local charge sectors. In the effective Hamiltonian picture, such charge reconfiguration is an off-resonant process. Changing the charge configuration across N_A sites requires virtually occupying intermediate states up the Stark ladder. According to high-order perturbation theory, the effective matrix element for a process spanning N_A sites scales as $J_{\text{eff}} \sim J(J/F)^{N_A-1}$. The timescale for symmetry restoration, and consequently the time scale on which the QME occurs, is inversely proportional to this rate:

$$t_M \propto \frac{1}{J_{\text{eff}}} \sim \frac{1}{J}\left(\frac{F}{J}\right)^{N_A-1}. \tag{24}$$

This prediction implies that the Mpemba time grows exponentially with the subsystem size N_A and follows a power-law dependence on the Stark field strength F. This confirms that the phenomenon is controlled by the localization length of the system, consistent with the numerical observations in Fig. 3(b) and Fig. 4(d).

3.2. Numerical Results

3.2.1. Stark Many-Body Localized Diagnostics

We first establish the parameter regime in which the tilted XXZ chain, described by the Hamiltonian in Eq. (1), enters the Stark-MBL phase. To obtain reliable information regarding the energy spectrum and eigenstates, we numerically solve the static and dynamical properties of the system using the Exact Diagonalization method. Fig. 2(a) shows the half-chain von Neumann entropy density

 doi:10.20944/preprints202602.1143.v1

$\overline{S_{N/2}}/N$ as a function of the Stark field F for several system sizes N. In the small-F regime, $\overline{S_{N/2}}/N$ remains finite and exhibits only a mild size dependence, consistent with the volume-law behavior of the ergodic phase. As F increases, $\overline{S_{N/2}}/N$ decreases substantially and drifts downward with increasing N, indicating a crossover toward the area-law entanglement characteristic of Stark-MBL. The inset of Fig. 2(a) demonstrates a finite-size scaling collapse as a function of $(F - F_c)N^{1/\nu}$, yielding a critical field $F_c \simeq 4.0$ (indicated by the vertical green dotted line). Based on this result, we use $F = 15 > F_c$ as a representative Stark-MBL point in our subsequent analysis.

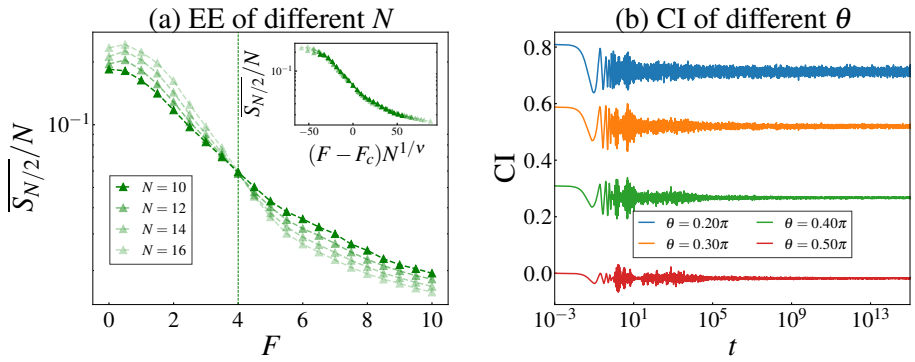

Figure 2. (a) The half-chain von Neumann entropy density $\overline{S_{N/2}}/N$ with different N. Inset in (a): finite-site scaling collapse of $\overline{S_{N/2}}/N$ as a function of $(F - F_c)N^{1/\nu}$, with the critical point $F_c \simeq 4.0$. (b) Charge imbalance dynamics with $N = 14$ and $F = 15 > F_c$. The initial state is chosen as TNS.

To further obtain dynamical evidence of non-ergodicity, we examine the charge imbalance $\mathrm{CI}(t)$ starting from the initial TNS. Fig. 2(b) plots the dynamics of $\mathrm{CI}(t)$ at $N = 14$ and $F = 15$ for several tilt angles θ. After an early-time transient, $\mathrm{CI}(t)$ rapidly approaches a non-zero long-time plateau. Crucially, the plateau value remains strongly dependent on the initial angle θ, preserving the ordering of the initial conditions over extremely long time scales (up to $t \sim 10^{15}$). This persistent memory of the initial staggered pattern provides direct dynamical evidence for the non-ergodicity protected by the Stark-MBL phase.

3.2.2. EA dynamics and the emergence of QME

Having established the phase diagram, we turn to the core objective: investigating the dynamics of the Rényi-2 EA $\Delta S_A^{(2)}(t)$ and the resulting QME. To explore how the initial state distribution affects the symmetry restoration process, we first analyze the microscopic composition of the initial states by calculating the charge-sector weights $p_A(q_A) = \mathrm{Tr}(\Pi_{q_A}\rho_A)$, where Π_{q_A} is the projection operator onto the eigenspace of the local charge operator $Q_A = \sum_{j\in A} S_j^z$ with eigenvalue q_A. To further characterize the spatial memory of the initial configurations, we calculate the charge imbalance (CI), which for our spin-$\frac{1}{2}$ system is defined as

$$\mathrm{CI}(t) = \frac{1}{N}\sum_{i=1}^{N}(-1)^i\langle S_i^z(t)\rangle. \tag{25}$$

Figs. 3(a) and 3(b) show the EA dynamics for the TNS at $F = 2$ and $F = 15$, respectively. At the ergodic point $F = 2$ [Fig. 3(a)], while larger θ corresponds to a larger initial EA, the ordering of the curves does not invert during relaxation, and the QME is absent. The inset shows that $p_A(q_A)$ for the TNS is nearly insensitive to θ. However, deep in the Stark-MBL regime ($F = 15$), the EA curves exhibit clears, signaling the emergence of the QME. In contrast, for the TFS at $F = 2$ [Fig. 4(a)], the QME is already observable, which is highly consistent with the microscopic feature shown in its inset where $p_A(q_A)$ significantly shifts toward the central sectors as θ increases.

 doi:10.20944/preprints202602.1143.v1

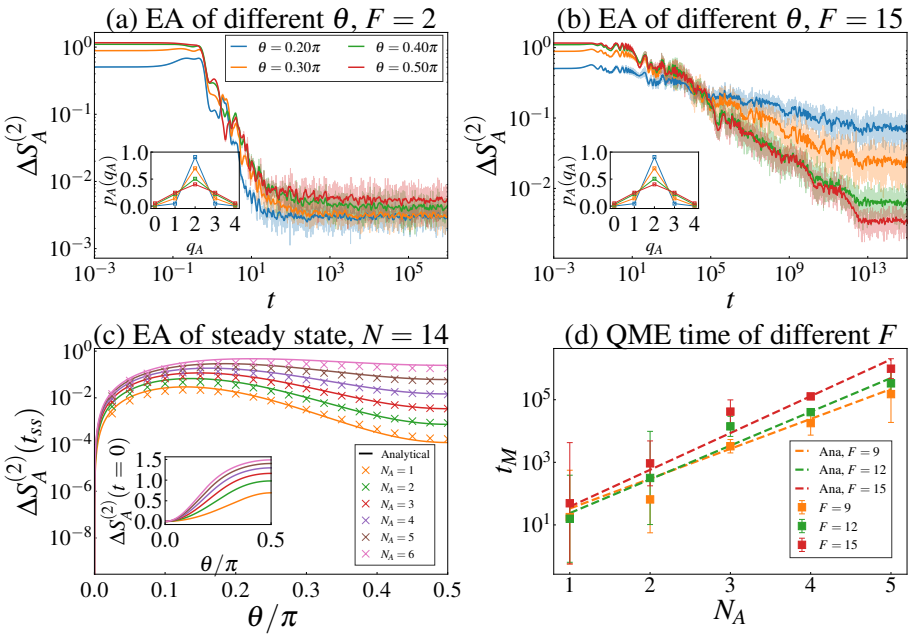

Figure 3. (a) and (b) EA dynamics with $N = 14$ and $N_A = 3$. The initial state is chosen as TNS. The numerical curves have been smoothed by convolution with a Gaussian, $\omega(n) = e^{-(n/\sigma)^2}$, with $\sigma = 5$. Inset in (a) and (b): Charge-sector weights $p_A(q_A)$ with $N = 14$ and $N_A = 4$, for the initial TNS. (c) Steady-state EA for $F = 15 > F_c$ and different subsystem sizes N_A, with the initial state prepared as the TNS. Discrete points show the steady-state EA averaged over 2000 samples, while solid lines denote the analytical steady-state values. Inset in (c): analytical initial EA at $t = 0$. (d) QME time t_M as a function of subsystem size N_A for different F at $N = 14$, starting from the initial TNS. Discrete symbols (with error bars) show the numerically extracted t_M, while dashed lines denote the theoretical scaling curves obtained by fitting Eq. (24) to the numerical data.

Then, to verify the accuracy of our aforementioned analytical predictions, we perform a quantitative comparison between the long-time numerical results and the analytical plateau values. In Fig. 3(c) (TNS) and Fig. 4(c) (TFS), we plot the steady-state EA $\Delta S_A^{(2)}(t_{\rm ss})$ versus θ/π for $F = 15$. The discrete symbols represent the numerical results averaged over 2000 samples, while the solid lines denote the analytical values. The results show that the numerical simulations and analytical predictions are in excellent agreement across all subsystem sizes N_A. This provides strong evidence that our analytical framework quantitatively reproduces the long-time dephasing behavior of Stark-MBL systems under symmetry constraints.

3.2.3. Scaling characteristics of the Mpemba time

Finally, we quantify the characteristic timescale of the QME. We define the Mpemba time t_M (corresponding to the first intersection of the EA dynamical envelopes) by extracting the first point of the EA curves and fit the numerical results using the analytically derived scaling relation Eq. (24). As shown in Fig. 3(d) and Fig. 4(d), the fitting curves (dashed lines) perfectly capture the exponential growth of t_M with respect to both subsystem size N_A and field strength F. This not only further validates the theoretical predictions but also reveals that in the Stark-MBL environment, the QME timescale is dominated by suppressed high-order operator dynamics, where the effective transition rate $J_{\rm eff}$ decays as $(J/F)^{N_A-1}$.

 doi:10.20944/preprints202602.1143.v1

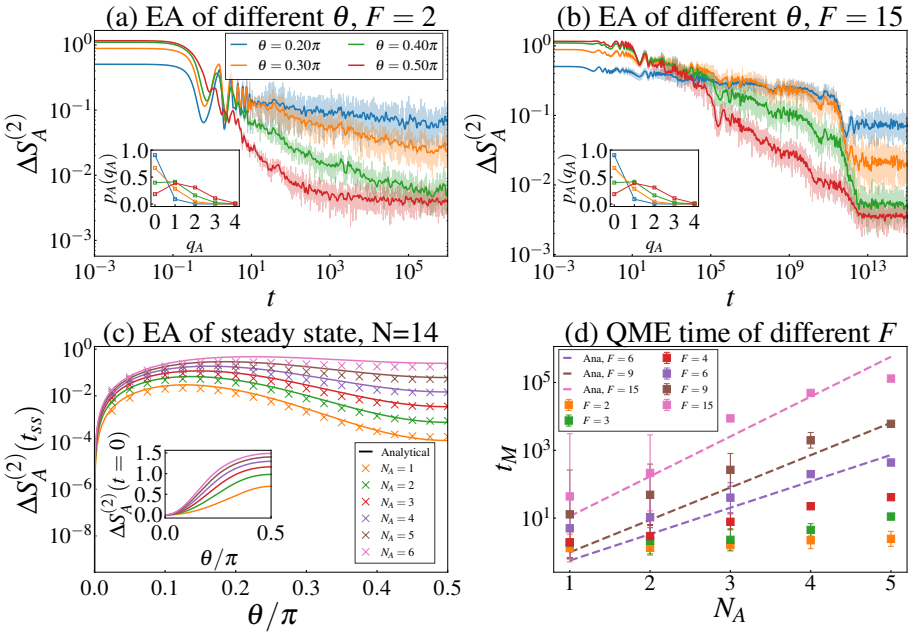

Figure 4. (a) and (b) EA dynamics with $N = 14$ and $N_A = 3$. The initial state is chosen as TFS. The numerical curves have been smoothed by convolution with a Gaussian, $\omega(n) = e^{-(n/\sigma)^2}$, with $\sigma = 5$. Inset in (a) and (b): Charge-sector weights $p_A(q_A)$ with $N = 14$ and $N_A = 4$, for the initial TFS. (c) Steady-state EA versus θ for $F = 15 > F_c$ and different subsystem sizes N_A, with the initial state prepared as the TFS. Discrete points show the steady-state EA averaged over late-time 2000 samples, while solid lines denote the analytical steady-state values. Inset in (c): analytical initial EA at $t = 0$. (d) QME time t_M as a function of subsystem size N_A for different F at $N = 14$, starting from the initial TFS. Discrete symbols (with error bars) show the numerically extracted t_M, while dashed lines denote the theoretical scaling curves obtained by fitting Eq. (24) to the numerical data.

4. Conclusions

To sum up, in this work, we have provided a comprehensive analysis of symmetry restoration and the QME within the context of Stark-MBL. By investigating the dynamics of the Rényi-2 EA in a tilted XXZ chain, we revealed that the Stark-induced breaking of ergodicity leads to a robust and universal Mpemba effect, distinct from its behavior in thermalizing systems.

Our central finding is that while the occurrence of the QME in the ergodic phase is contingent upon the specific choice of the initial state (e.g., present for TFS but absent for TNS), the Stark-MBL regime enforces a universal inversion of relaxation hierarchies. Through an analytical operator-string expansion, we demonstrated that this universality stems from the structure of the steady-state EA. In the strong-tilt limit, the effective Hilbert space dimension accessible to local observables is strictly constrained by the Stark potential, leading to a "hotter-is-faster" relaxation scenario where states with larger initial asymmetry ultimately approach a more symmetric steady state. Furthermore, we established that the timescale of this anomalous relaxation, the Mpemba time t_M, is governed by high-order off-resonant processes. We derived a scaling law showing that t_M grows exponentially with the subsystem size and follows a power-law dependence on the field strength. This prediction is fully supported by our numerical simulations, confirming that symmetry restoration in Stark-MBL is driven by slow, perturbative quantum fluctuations rather than diffusive transport. Our results highlight the unique potential of Stark-MBL systems as tunable platforms for exploring non-equilibrium thermodynamics and symmetry dynamics. Unlike disorder-driven MBL, the Stark potential offers a clean, continuously adjustable control parameter to engineer relaxation pathways. This suggests promising avenues for observing the QME in present-day quantum simulators, such as cold atoms [75–81] in optical lattices or trapped ions [82], where linear potentials can be implemented with high precision.

Finally, our study opens up several specific directions for future theoretical investigation. While we focused on closed quantum systems, examining the stability of the Mpemba effect under dissipative or non-Hermitian dynamics [83–98] would be crucial for understanding its fate in realistic open

 doi:10.20944/preprints202602.1143.v1

environments. Additionally, extending the analysis to the framework of nonstabilizerness [99–154] offers a fresh perspective. Utilizing metrics such as the stabilizer Rényi entropy as dynamical probes could quantify the complexity of the relaxation process, potentially revealing a rich interplay between symmetry restoration, localization, and the scrambling of quantum magic.

Author Contributions: J.X.Z. conceived and designed the project. H.Z.L. performed the analytical calculations. Y.R.Z. provided the code for the numerical simulations. H.Z.L. and Y.R.Z. equally contributed to the writing.

Funding: J.X.Z. was supported by the National Natural Science Foundation of China (Grant Nos. 12374046 and 11874316), the Shanghai Science and Technology Innovation Action Plan (Grant No. 24LZ1400800), the National Basic Research Program of China (Grant No. 2015CB921103), and the Program for Changjiang Scholars and Innovative Research Teams in Universities (Grant No. IRT13093). H.Z.L. is supported by a China Scholarship Council Scholarship (Grant No. 202506890103).

Data Availability Statement: The data sets generated and/or analyzed during the current study are available from the corresponding authors upon reasonable request.

Acknowledgments: We thank Dr. Shuo Liu and Prof. Shi-Xin Zhang for the helpful and valuable discussions. H.Z.L. also appreciate Ching Hua Lee for the guidance.

Conflicts of Interest: The authors declare no conflicts of interest.

Appendix A. Additional Numerical Results

To further clarify where the QME occurs in parameter space, we provide a "Phase diagram" of the presence or absence of QME in the (F, θ_2) plane for the TNS at fixed $\theta_1 = 0.2\pi$ (Fig. A1), obtained from a systematic survey of the EA dynamics.

We map out a "Phase diagram" of the presence or absence of QME in the (F, θ_2) plane at fixed $\theta_1 = 0.2\pi$ for the initial TNS (Fig. A1) with $N = 12$ and $N_A = 3$. For each pair (F, θ_2), we compute the EA dynamics following the same procedure as in the main text and inspect the evolution of $\Delta S_A^{(2)}(t)$. After smoothing out the fast Stark-induced oscillations, we determine for each (F, θ_2) whether QME is present according to the criterion defined in the main text, and label the point as "with QME" or "without QME" accordingly. Near the crossover, the can be weak or ambiguous within finite-size numerics, and the blue error bars indicate the corresponding uncertainty in locating the approximate boundary.

Overall, the QME for the TNS is absent at small F but becomes clearly visible beyond a characteristic scale around $F \simeq 4$, consistent with the main text, where no QME is found at small F whereas a clear QME is observed at large F.

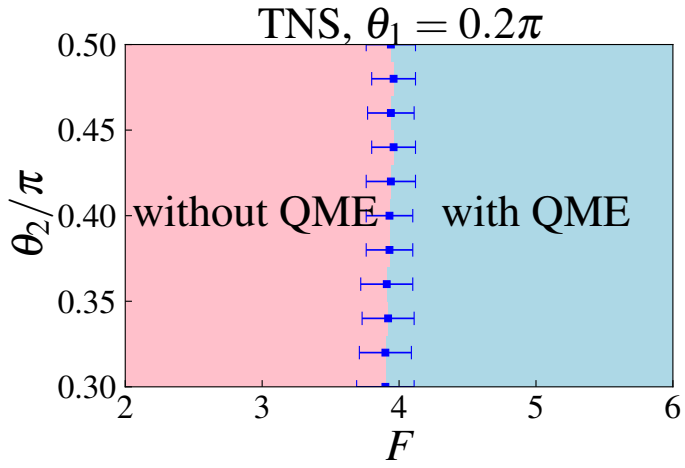

Figure A1. "Phase diagram" of the presence or absence of QME in the (F, θ_2) plane at fixed $\theta_1 = 0.2\pi$ for the initial TNS. Light-blue (pink) indicates parameter sets with (without) QME. Blue error bars mark the uncertainty of the crossover boundary within our finite-size numerics. Here $N = 12$ and $N_A = 3$.

 doi:10.20944/preprints202602.1143.v1

References

1. D'Alessio, L.; Kafri, Y.; Polkovnikov, A.; Rigol, M. From quantum chaos and eigenstate thermalization to statistical mechanics and thermodynamics. *Advances in Physics* **2016**, *65*, 239–362. https://doi.org/10.1080/00018732.2016.1198134.
2. Liu, Z.W.; Lloyd, S.; Zhu, E.; Zhu, H. Entanglement, quantum randomness, and complexity beyond scrambling. *Journal of High Energy Physics* **2018**, *2018*, 41. https://doi.org/10.1007/JHEP07(2018)041.
3. Srednicki, M. Chaos and quantum thermalization. *Phys. Rev. E* **1994**, *50*, 888–901. https://doi.org/10.1103/PhysRevE.50.888.
4. Deutsch, J.M. Quantum statistical mechanics in a closed system. *Phys. Rev. A* **1991**, *43*, 2046–2049. https://doi.org/10.1103/PhysRevA.43.2046.
5. Wiseman, H.M.; Vaccaro, J.A. Entanglement of Indistinguishable Particles Shared between Two Parties. *Phys. Rev. Lett.* **2003**, *91*, 097902. https://doi.org/10.1103/PhysRevLett.91.097902.
6. Popescu, S.; Short, A.J.; Winter, A. Entanglement and the foundations of statistical mechanics. *Nature Physics* **2006**, *2*, 754–758. https://doi.org/10.1038/nphys444.
7. Russotto, A.; Ares, F.; Calabrese, P. Symmetry breaking in chaotic many-body quantum systems at finite temperature. *Phys. Rev. E* **2025**, *112*, L032101. https://doi.org/10.1103/kppn-3272.
8. Chang, R.A.; Shrotriya, H.; Ho, W.W.; Ippoliti, M. Deep Thermalization under Charge-Conserving Quantum Dynamics. *PRX Quantum* **2025**, *6*, 020343. https://doi.org/10.1103/PRXQuantum.6.020343.
9. Yamashika, S.; Calabrese, P.; Ares, F. Quenching from superfluid to free bosons in two dimensions: Entanglement, symmetries, and the quantum Mpemba effect. *Phys. Rev. A* **2025**, *111*, 043304. https://doi.org/10.1103/PhysRevA.111.043304.
10. Klobas, K.; Rylands, C.; Bertini, B. Translation symmetry restoration under random unitary dynamics. *Phys. Rev. B* **2025**, *111*, L140304. https://doi.org/10.1103/PhysRevB.111.L140304.
11. Banerjee, T.; Das, S.; Sengupta, K. Entanglement asymmetry in periodically driven quantum systems. *SciPost Phys.* **2025**, *19*, 051. https://doi.org/10.21468/SciPostPhys.19.2.051.
12. Kusuki, Y.; Murciano, S.; Ooguri, H.; Pal, S. Entanglement asymmetry and symmetry defects in boundary conformal field theory. *J. High Energy Phys.* **2025**, *2025*, 57. https://doi.org/10.1007/JHEP01(2025)057.
13. Lastres, M.; Murciano, S.; Ares, F.; Calabrese, P. Entanglement asymmetry in the critical XXZ spin chain. J. Stat. Mech. (2025) 013107.
14. Rylands, C.; Vernier, E.; Calabrese, P. Dynamical symmetry restoration in the Heisenberg spin chain. J. Stat. Mech. (2024) 123102.
15. Chalas, K.; Ares, F.; Rylands, C.; Calabrese, P. Multiple crossings during dynamical symmetry restoration and implications for the quantum Mpemba effect. J. Stat. Mech. (2024) 103101.
16. Ares, F.; Murciano, S.; Calabrese, P. Entanglement asymmetry as a probe of symmetry breaking. *Nat. Commun.* **2023**, *14*, 2036. https://doi.org/10.1038/s41467-023-37747-8.
17. Ares, F.; Calabrese, P.; Murciano, S. The quantum Mpemba effects. *Nat. Rev. Phys.* **2025**, *7*, 451–460.
18. Yu, H.; Liu, S.; Zhang, S.X. Quantum Mpemba effects from symmetry perspectives. *AAPPS Bulletin* **2025**, *35*, 17.
19. Chatterjee, A.K.; Takada, S.; Hayakawa, H. Quantum Mpemba Effect in a Quantum Dot with Reservoirs. *Phys. Rev. Lett.* **2023**, *131*, 080402. https://doi.org/10.1103/PhysRevLett.131.080402.
20. Aharony Shapira, S.; Shapira, Y.; Markov, J.; Teza, G.; Akerman, N.; Raz, O.; Ozeri, R. Inverse Mpemba Effect Demonstrated on a Single Trapped Ion Qubit. *Phys. Rev. Lett.* **2024**, *133*, 010403. https://doi.org/10.1103/PhysRevLett.133.010403.
21. Di Giulio, G.; Turkeshi, X.; Murciano, S. Measurement-Induced Symmetry Restoration and Quantum Mpemba Effect. *Entropy* **2025**, *27*, 407. https://doi.org/10.3390/e27040407.
22. Westhoff, P.; Paeckel, S.; Moroder, M. Fast and direct preparation of a genuine lattice BEC via the quantum Mpemba effect. *arXiv:2504.05549* **2025**.
23. Guo, S.; Yin, S.; Zhang, S.X.; Li, Z.X. Skin Effect Induced Anomalous Dynamics from Charge-Fluctuating Initial States. *arXiv:2504.21631* **2025**.
24. Longhi, S. Quantum Mpemba effect from initial system-reservoir entanglement. *arXiv:2504.21758* **2025**.
25. Xu, M.; Wei, Z.; Jiang, X.P.; Pan, L. Expedited thermalization dynamics in incommensurate systems. *Phys. Rev. A* **2025**, *112*, 042210. https://doi.org/10.1103/9qkm-35y1.
26. Nava, A.; Egger, R. Pontus-Mpemba Effects. *Phys. Rev. Lett.* **2025**, *135*, 140404. https://doi.org/10.1103/hhgj-89gj.

 doi:10.20944/preprints202602.1143.v1

27. Ramon-Escandell, C.; Prositto, A.; Segal, D. Thermal state preparation by repeated interactions at and beyond the Lindblad limit. *arXiv:2506.12166* **2025**.
28. Summer, A.; Moroder, M.; Bettmann, L.P.; Turkeshi, X.; Marvian, I.; Goold, J. A resource theoretical unification of Mpemba effects: classical and quantum. *arXiv:2507.16976* **2025**.
29. Ma, W.; Liu, J. Quantum Mpemba effect in parity-time symmetric systems. *arXiv:2508.17575* **2025**.
30. Nava, A.; Fabrizio, M. Lindblad dissipative dynamics in the presence of phase coexistence. *Phys. Rev. B* **2019**, *100*, 125102. https://doi.org/10.1103/PhysRevB.100.125102.
31. Chatterjee, A.K.; Takada, S.; Hayakawa, H. Multiple quantum Mpemba effect: Exceptional points and oscillations. *Phys. Rev. A* **2024**, *110*, 022213. https://doi.org/10.1103/PhysRevA.110.022213.
32. Kochsiek, S.; Carollo, F.; Lesanovsky, I. Accelerating the approach of dissipative quantum spin systems towards stationarity through global spin rotations. *Phys. Rev. A* **2022**, *106*, 012207. https://doi.org/10.1103/PhysRevA.106.012207.
33. Carollo, F.; Lasanta, A.; Lesanovsky, I. Exponentially Accelerated Approach to Stationarity in Markovian Open Quantum Systems through the Mpemba Effect. *Phys. Rev. Lett.* **2021**, *127*, 060401. https://doi.org/10.1103/PhysRevLett.127.060401.
34. Ivander, F.; Anto-Sztrikacs, N.; Segal, D. Hyperacceleration of quantum thermalization dynamics by bypassing long-lived coherences: An analytical treatment. *Phys. Rev. E* **2023**, *108*, 014130. https://doi.org/10.1103/PhysRevE.108.014130.
35. Shapira, S.A.; Shapira, Y.; Markov, J.; Teza, G.; Akerman, N.; Raz, O.; Ozeri, R. The inverse Mpemba effect demonstrated on a single trapped ion qubit. *arXiv:2401.05830* **2024**.
36. Strachan, D.J.; Purkayastha, A.; Clark, S.R. Non-Markovian Quantum Mpemba effect. *arXiv:2402.05756* **2024**.
37. Wang, X.; Wang, J. Mpemba effects in nonequilibrium open quantum systems. *Phys. Rev. Res.* **2024**, *6*, 033330. https://doi.org/10.1103/PhysRevResearch.6.033330.
38. Moroder, M.; Culhane, O.; Zawadzki, K.; Goold, J. Thermodynamics of the Quantum Mpemba Effect. *Phys. Rev. Lett.* **2024**, *133*, 140404. https://doi.org/10.1103/PhysRevLett.133.140404.
39. Kochsiek, S.; Carollo, F.; Lesanovsky, I. Accelerating the approach of dissipative quantum spin systems towards stationarity through global spin rotations. *Phys. Rev. A* **2022**, *106*, 012207. https://doi.org/10.1103/PhysRevA.106.012207.
40. Carollo, F.; Lasanta, A.; Lesanovsky, I. Exponentially Accelerated Approach to Stationarity in Markovian Open Quantum Systems through the Mpemba Effect. *Phys. Rev. Lett.* **2021**, *127*, 060401. https://doi.org/10.1103/PhysRevLett.127.060401.
41. Ivander, F.; Anto-Sztrikacs, N.; Segal, D. Hyperacceleration of quantum thermalization dynamics by bypassing long-lived coherences: An analytical treatment. *Phys. Rev. E* **2023**, *108*, 014130. https://doi.org/10.1103/PhysRevE.108.014130.
42. Ares, F.; Vitale, V.; Murciano, S. Quantum Mpemba effect in free-fermionic mixed states. *Phys. Rev. B* **2025**, *111*, 104312. https://doi.org/10.1103/PhysRevB.111.104312.
43. Dong, J.W.; Mu, H.F.; Qin, M.; Cui, H.T. Quantum Mpemba effect of localization in the dissipative mosaic model. *Phys. Rev. A* **2025**, *111*, 022215. https://doi.org/10.1103/PhysRevA.111.022215.
44. Longhi, S. Quantum Mpemba Effect from Non-Normal Dynamics. *Entropy* **2025**, *27*, 581. https://doi.org/10.3390/e27060581.
45. Wang, Y. Non-Markovian quantum Mpemba effect in strongly correlated quantum dots. *arXiv:2510.23445* **2025**.
46. Bagui, P.; Chatterjee, A.; Agarwalla, B.K. Accelerated relaxation and Mpemba-like effect for operators in open quantum systems. *arXiv:2510.24630* **2025**.
47. Zhang, Z.Z.; Luo, H.G.; Wu, W. Quantum Mpemba Effect Induced by Non-Markovian Exceptional Point. *arXiv:2511.13173* **2025**.
48. Qian, D.; Wang, H.; Wang, J. Intrinsic quantum Mpemba effect in Markovian systems and quantum circuits. *Phys. Rev. B* **2025**, *111*, L220304. https://doi.org/10.1103/qj8n-k5j2.
49. Yu, Y.H.; Jin, T.R.; Zhang, L.; Xu, K.; Fan, H. Tuning the quantum Mpemba effect in an isolated system by initial-state engineering. *Phys. Rev. B* **2025**, *112*, 094315. https://doi.org/10.1103/yzjd-pk8h.
50. Bhore, T.; Su, L.; Martin, I.; Clerk, A.A.; Papić, Z. Quantum Mpemba effect without global symmetries. *Phys. Rev. B* **2025**, *112*, L121109. https://doi.org/10.1103/1td3-2vwf.
51. Gibbins, M.; Smith, A.; Bertini, B. Translation symmetry restoration in integrable systems: the noninteracting case. *arXiv:2506.14555* **2025**.

 doi:10.20944/preprints202602.1143.v1

52. Sugimoto, K.; Kuwahara, T.; Saito, K. Prethermal inverse Mpemba effect. *arXiv:2507.04669* **2025**.
53. Ares, F.; Rylands, C.; Calabrese, P. A simpler probe of the quantum Mpemba effect in closed systems. *arXiv:2507.05946* **2025**.
54. Yamashika, S.; Ares, F. The quantum Mpemba effect in long-range spin systems. *arXiv:2507.06636* **2025**.
55. Zhao, M.; Hou, Z. Noise-induced Quantum Mpemba effect. *arXiv:2507.11915* **2025**.
56. Xu, Y.; Fang, C.P.; Chen, B.J.; Wang, M.C.; Ge, Z.Y.; Shi, Y.H.; Liu, Y.; Deng, C.L.; Zhao, K.; Liu, Z.H.; et al. Observation and Modulation of the Quantum Mpemba Effect on a Superconducting Quantum Processor. *arXiv:2508.07707* **2025**.
57. Wei, Z.; Xu, M.; Jiang, X.P.; Hu, H.; Pan, L. Quantum Mpemba Effect in Dissipative Spin Chains at Criticality. *arXiv:2508.18906* **2025**.
58. Yu, H.; Hu, J.; Zhang, S.X. Quantum Pontus-Mpemba Effects in Real and Imaginary-time Dynamics. *arXiv:2509.01960* **2025**.
59. Aditya, S.; Summer, A.; Sierant, P.; Turkeshi, X. Mpemba Effects in Quantum Complexity. *arXiv:2509.22176* **2025**.
60. Cao, S.; Ge, X.H. Symmetry restoration in a fast scrambling system. *arXiv:2509.26176* **2025**.
61. Liu, S.; Zhang, H.K.; Yin, S.; Zhang, S.X. Symmetry Restoration and Quantum Mpemba Effect in Symmetric Random Circuits. *Phys. Rev. Lett.* **2024**, *133*, 140405. https://doi.org/10.1103/PhysRevLett.133.140405.
62. Liu, S.; Zhang, H.K.; Yin, S.; Zhang, S.X.; Yao, H. Symmetry restoration and quantum Mpemba effect in many-body localization systems. *Science Bulletin* **2025**. https://doi.org/10.1016/j.scib.2025.10.017.
63. Turkeshi, X.; Calabrese, P.; De Luca, A. Quantum Mpemba Effect in Random Circuits. *Phys. Rev. Lett.* **2025**, *135*, 040403. https://doi.org/10.1103/PhysRevLett.135.040403.
64. Yamashika, S.; Ares, F.; Calabrese, P. Entanglement asymmetry and quantum Mpemba effect in two-dimensional free-fermion systems. *Phys. Rev. B* **2024**, *110*, 085126. https://doi.org/10.1103/PhysRevB.110.085126.
65. Ares, F.; Murciano, S.; Vernier, E.; Calabrese, P. Lack of symmetry restoration after a quantum quench: An entanglement asymmetry study. *SciPost Phys.* **2023**, *15*, 089. https://doi.org/10.21468/SciPostPhys.15.3.089.
66. Bertini, B.; Klobas, K.; Collura, M.; Calabrese, P.; Rylands, C. Dynamics of charge fluctuations from asymmetric initial states. *Phys. Rev. B* **2024**, *109*, 184312. https://doi.org/10.1103/PhysRevB.109.184312.
67. Yamashika, S.; Ares, F.; Calabrese, P. Entanglement asymmetry and quantum Mpemba effect in two-dimensional free-fermion systems. *Phys. Rev. B* **2024**, *110*, 085126. https://doi.org/10.1103/PhysRevB.110.085126.
68. Alishahiha, M.; Vasli, M.J. On Krylov Complexity as a Probe of the Quantum Mpemba Effect. *arXiv:2510.14740* **2025**.
69. Russotto, A.; Ares, F.; Calabrese, P.; Alba, V. Dynamics of entanglement fluctuations and quantum Mpemba effect in the $\nu = 1$ QSSEP model. *arXiv:2510.25519* **2025**.
70. Li, H.Z.; Lee, C.H.; Liu, S.; Zhang, S.X.; Zhong, J.X. Quantum Mpemba effect in long-ranged U(1)-symmetric random circuits. *arXiv:2512.06775* **2025**.
71. Abanin, D.A.; Altman, E.; Bloch, I.; Serbyn, M. Colloquium: Many-body localization, thermalization, and entanglement. *Rev. Mod. Phys.* **2019**, *91*, 021001. https://doi.org/10.1103/RevModPhys.91.021001.
72. Schulz, M.; Hooley, C.A.; Moessner, R.; Pollmann, F. Stark Many-Body Localization. *Physical Review Letters* **2019**, *122*, 040606. https://doi.org/10.1103/PhysRevLett.122.040606.
73. van Nieuwenburg, E.; Baum, Y.; Refael, G. From Bloch oscillations to many-body localization in clean interacting systems. *Proceedings of the National Academy of Sciences* **2019**, *116*, 9269–9274. https://doi.org/10.1073/pnas.1819316116.
74. Morong, W.; Liu, F.; Becker, P.; Collins, K.S.; Feng, L.; Kyprianidis, A.; Pagano, G.; You, T.; Gorshkov, A.V.; Monroe, C. Observation of Stark many-body localization without disorder. *Nature* **2021**, *599*, 393–398. https://doi.org/10.1038/s41586-021-03988-0.
75. Ebadi, S.; Wang, T.T.; Levine, H.; Keesling, A.; Semeghini, G.; Omran, A.; Bluvstein, D.; Samajdar, R.; Pichler, H.; Ho, W.W.; et al. Quantum phases of matter on a 256-atom programmable quantum simulator. *Nature* **2021**, *595*, 227–232. https://doi.org/10.1038/s41586-021-03582-4.
76. Semeghini, G.; Levine, H.; Keesling, A.; Ebadi, S.; Wang, T.T.; Bluvstein, D.; Verresen, R.; Pichler, H.; Kalinowski, M.; Samajdar, R.; et al. Probing topological spin liquids on a programmable quantum simulator. *Science* **2021**, *374*, 1242–1247. https://doi.org/10.1126/science.abi8794.

 doi:10.20944/preprints202602.1143.v1

77. Ebadi, S.; Keesling, A.; Cain, M.; Wang, T.T.; Levine, H.; Bluvstein, D.; Semeghini, G.; Omran, A.; Liu, J.G.; Samajdar, R.; et al. Quantum optimization of maximum independent set using Rydberg atom arrays. *Science* **2022**, *376*, 1209–1215. https://doi.org/10.1126/science.abo6587.
78. Bluvstein, D.; Levine, H.; Semeghini, G.; Wang, T.T.; Ebadi, S.; Kalinowski, M.; Keesling, A.; Maskara, N.; Pichler, H.; Greiner, M.; et al. A quantum processor based on coherent transport of entangled atom arrays. *Nature* **2022**, *604*, 451–456. https://doi.org/10.1038/s41586-022-04592-6.
79. Evered, S.J.; Bluvstein, D.; Kalinowski, M.; Ebadi, S.; Manovitz, T.; Zhou, H.; Li, S.H.; Geim, A.A.; Wang, T.T.; Maskara, N.; et al. High-fidelity parallel entangling gates on a neutral-atom quantum computer. *Nature* **2023**, *622*, 268–272. https://doi.org/10.1038/s41586-023-06481-y.
80. Bluvstein, D.; Evered, S.J.; Geim, A.A.; Li, S.H.; Zhou, H.; Manovitz, T.; Ebadi, S.; Cain, M.; Kalinowski, M.; Hangleiter, D.; et al. Logical quantum processor based on reconfigurable atom arrays. *Nature* **2024**, *626*, 58–65. https://doi.org/10.1038/s41586-023-06927-3.
81. Shen, R.; Chen, T.; Aliyu, M.M.; Qin, F.; Zhong, Y.; Loh, H.; Lee, C.H. Proposal for Observing Yang-Lee Criticality in Rydberg Atomic Arrays. *Phys. Rev. Lett.* **2023**, *131*, 080403.
82. Joshi, L.K.; Franke, J.; Rath, A.; Ares, F.; Murciano, S.; Kranzl, F.; Blatt, R.; Zoller, P.; Vermersch, B.; Calabrese, P.; et al. Observing the Quantum Mpemba Effect in Quantum Simulations. *Phys. Rev. Lett.* **2024**, *133*, 010402. https://doi.org/10.1103/PhysRevLett.133.010402.
83. El-Ganainy, R.; Makris, K.G.; Khajavikhan, M.; Musslimani, Z.H.; Rotter, S.; Christodoulides, D.N. Non-Hermitian physics and PT symmetry. *Nature Physics* **2018**, *14*, 11. https://doi.org/10.1038/nphys4323.
84. Bergholtz, E.J.; Budich, J.C.; Kunst, F.K. Exceptional topology of non-Hermitian systems. *Reviews of Modern Physics* **2021**, *93*, 015005. https://doi.org/10.1103/RevModPhys.93.015005.
85. Ashida, Y.; Gong, Z.; Ueda, M. Non-Hermitian physics. *Advances in Physics* **2020**, *69*, 249–435. https://doi.org/10.1080/00018732.2020.1786435.
86. Heiss, W.D. The physics of exceptional points. *Journal of Physics A: Mathematical and Theoretical* **2012**, *45*, 444016. https://doi.org/10.1088/1751-8113/45/44/444016.
87. Lee, C.H.; Thomale, R. Anatomy of skin modes and topology in non-Hermitian systems. *Physical Review B* **2019**, *99*, 201103. https://doi.org/10.1103/PhysRevB.99.201103.
88. Yu, X.J.; Pan, Z.; Xu, L.; Li, Z.X. Non-Hermitian Strongly Interacting Dirac Fermions. *Phys. Rev. Lett.* **2024**, *132*, 116503. https://doi.org/10.1103/PhysRevLett.132.116503.
89. Chen, W.; Özdemir, Ş.K.; Zhao, G.; Wiersig, J.; Yang, L. Exceptional points enhance sensing in an optical microcavity. *Nature* **2017**, *548*, 192. https://doi.org/10.1038/nature23281.
90. Lau, H.W.; Clerk, A.A. Fundamental limits and non-reciprocal approaches in non-Hermitian quantum sensing. *Nature Communications* **2018**, *9*, 4320. https://doi.org/10.1038/s41467-018-06477-7.
91. Li, S.Z.; Li, Z. Ring structure in the complex plane: A fingerprint of a non-Hermitian mobility edge. *Phys. Rev. B* **2024**, *110*, L041102. https://doi.org/10.1103/PhysRevB.110.L041102.
92. Liu, G.J.; Zhang, J.M.; Li, S.Z.; Li, Z. Emergent strength-dependent scale-free mobility edge in a nonreciprocal long-range Aubry-André-Harper model. *Phys. Rev. A* **2024**, *110*, 012222. https://doi.org/10.1103/PhysRevA.110.012222.
93. Yao, S.; Wang, Z. Edge states and topological invariants of non-Hermitian systems. *Physical Review Letters* **2018**, *121*, 086803. https://doi.org/10.1103/PhysRevLett.121.086803.
94. Chen, T.; Shen, R.; Lee, C.H.; Yang, B. High-fidelity realization of the AKLT state on a NISQ-era quantum processor. *SciPost Phys.* **2023**, *15*, 170. https://doi.org/10.21468/SciPostPhys.15.4.170.
95. Shen, R.; Chen, T.; Yang, B.; Lee, C.H., 2023. arXiv:2311.10143 [quant-ph].
96. Chen, T.; Shen, R.; Lee, C.H.; Yang, B. High-fidelity realization of the AKLT state on a NISQ-era quantum processor. *SciPost Phys.* **2023**, *15*, 170. https://doi.org/10.21468/SciPostPhys.15.4.170.
97. Lee, C.H.; Li, L.; Gong, J. Hybrid Higher-Order Skin-Topological Modes in Nonreciprocal Systems. *Phys. Rev. Lett.* **2019**, *123*, 016805. https://doi.org/10.1103/PhysRevLett.123.016805.
98. Lee, C.H.; Li, L.; Thomale, R.; Gong, J. Unraveling non-Hermitian pumping: Emergent spectral singularities and anomalous responses. *Phys. Rev. B* **2020**, *102*, 085151. https://doi.org/10.1103/PhysRevB.102.085151.
99. Chitambar, E.; Gour, G. Quantum resource theories. *Rev. Mod. Phys.* **2019**, *91*, 025001. https://doi.org/10.1103/RevModPhys.91.025001.
100. Liu, Z.W.; Winter, A. Many-Body Quantum Magic. *PRX Quantum* **2022**, *3*, 020333. https://doi.org/10.1103/PRXQuantum.3.020333.
101. Leone, L.; Oliviero, S.F.; Hamma, A. Stabilizer Rényi Entropy. *Physical Review Letters* **2022**, *128*, 050402. https://doi.org/10.1103/physrevlett.128.050402.

 doi:10.20944/preprints202602.1143.v1

102. Leone, L.; Bittel, L. Stabilizer entropies are monotones for magic-state resource theory. *Phys. Rev. A* **2024**, *110*, L040403. https://doi.org/10.1103/PhysRevA.110.L040403.
103. Tirrito, E.; Tarabunga, P.S.; Lami, G.; Chanda, T.; Leone, L.; Oliviero, S.F.E.; Dalmonte, M.; Collura, M.; Hamma, A. Quantifying nonstabilizerness through entanglement spectrum flatness. *Phys. Rev. A* **2024**, *109*, L040401. https://doi.org/10.1103/PhysRevA.109.L040401.
104. Turkeshi, X.; Schirò, M.; Sierant, P. Measuring nonstabilizerness via multifractal flatness. *Physical Review A* **2023**, *108*, 042408. https://doi.org/10.1103/physreva.108.042408.
105. Turkeshi, X.; Dymarsky, A.; Sierant, P. Pauli spectrum and nonstabilizerness of typical quantum many-body states. *Phys. Rev. B* **2025**, *111*, 054301. https://doi.org/10.1103/PhysRevB.111.054301.
106. Turkeshi, X.; Tirrito, E.; Sierant, P. Magic spreading in random quantum circuits. *Nat. Commun.* **2025**, *16*, 2575. https://doi.org/10.1038/s41467-025-57704-x.
107. Jasser, B.; Odavić, J.; Hamma, A. Stabilizer Entropy and entanglement complexity in the Sachdev-Ye-Kitaev model. *arXiv:2502.03093* **2025**.
108. Viscardi, M.; Dalmonte, M.; Hamma, A.; Tirrito, E. Interplay of entanglement structures and stabilizer entropy in spin models. *arXiv:2503.08620* **2025**.
109. Iannotti, D.; Esposito, G.; Campos Venuti, L.; Hamma, A. Entanglement and Stabilizer entropies of random bipartite pure quantum states. *Quantum* **2025**, *9*, 1797. https://doi.org/10.22331/q-2025-07-21-1797.
110. Cusumano, S.; Venuti, L.C.; Cepollaro, S.; Esposito, G.; Iannotti, D.; Jasser, B.; c, J.O.; Viscardi, M.; Hamma, A. Non-stabilizerness and violations of CHSH inequalities. *arXiv:2504.03351* **2025**.
111. Bittel, L.; Leone, L. Operational interpretation of the Stabilizer Entropy. *arXiv:2507.22883* **2025**.
112. Varikuti, N.D.; Bandyopadhyay, S.; Hauke, P. Impact of Clifford operations on non-stabilizing power and quantum chaos. *arXiv:2505.14793* **2025**.
113. Tirrito, E.; Turkeshi, X.; Sierant, P. Anticoncentration and nonstabilizerness spreading under ergodic quantum dynamics. *arXiv:2412.10229* **2025**.
114. Zhang, P.; Zhou, S.; Sun, N. Stabilizer Rényi Entropy and its Transition in the Coupled Sachdev-Ye-Kitaev Model. *arXiv:2509.17417* **2025**.
115. Qian, D.; Wang, J. Quantum nonlocal nonstabilizerness. *Phys. Rev. A* **2025**, *111*, 052443. https://doi.org/10.1103/PhysRevA.111.052443.
116. Moca, C.P.; Sticlet, D.; Dóra, B.; Valli, A.; Szombathy, D.; Zaránd, G. Non-stabilizerness generation in a multi-particle quantum walk. *arXiv:2504.19750* **2025**.
117. Dowling, N.; Kos, P.; Turkeshi, X. Magic Resources of the Heisenberg Picture. *Phys. Rev. Lett.* **2025**, *135*, 050401. https://doi.org/10.1103/p7xt-s9nz.
118. Bera, S.; Schirò, M. Non-Stabilizerness of Sachdev-Ye-Kitaev Model. *arXiv:2502.01582* **2025**.
119. Masot-Llima, S.; Garcia-Saez, A. Stabilizer Tensor Networks: Universal Quantum Simulator on a Basis of Stabilizer States. *Phys. Rev. Lett.* **2024**, *133*, 230601. https://doi.org/10.1103/PhysRevLett.133.230601.
120. Aditya, S.; Summer, A.; Sierant, P.; Turkeshi, X. Mpemba Effects in Quantum Complexity. *arXiv:2509.22176* **2025**.
121. Hernández-Yanes, T.; Sierant, P.; Zakrzewski, J.; Płodzień, M. Non-stabilizerness in quantum-enhanced metrological protocols. *arXiv:2510.01380* **2025**.
122. Falcão, P.R.N.; Sierant, P.; Zakrzewski, J.; Tirrito, E. Magic dynamics in many-body localized systems. *arXiv:2503.07468* **2025**.
123. Sticlet, D.; Dóra, B.; Szombathy, D.; Zaránd, G.; Moca, C.P. Non-stabilizerness in open XXZ spin chains: Universal scaling and dynamics. *arXiv:2504.11139* **2025**.
124. Tirrito, E.; Tarabunga, P.S.; Bhakuni, D.S.; Dalmonte, M.; Sierant, P.; Turkeshi, X. Universal Spreading of Nonstabilizerness and Quantum Transport. *arXiv:2506.12133* **2025**.
125. Zhang, Y.; Gu, Y. Quantum magic dynamics in random circuits. *arXiv:2410.21128* **2024**.
126. Cao, C.; Cheng, G.; Hamma, A.; Leone, L.; Munizzi, W.; Oliviero, S.F.E. Gravitational back-reaction is magical. *arXiv:2403.07056* **2025**.
127. Tarabunga, P.S.; Castelnovo, C. Magic in generalized Rokhsar-Kivelson wavefunctions. *Quantum* **2024**, *8*, 1347. https://doi.org/10.22331/q-2024-05-14-1347.
128. Qian, X.; Huang, J.; Qin, M. Augmenting a finite-temperature tensor network with Clifford circuits. *Phys. Rev. B* **2025**, *112*, 115150. https://doi.org/10.1103/gljy-1ykf.
129. Qian, X.; Huang, J.; Qin, M. Clifford Circuits Augmented Time-Dependent Variational Principle. *Phys. Rev. Lett.* **2025**, *134*, 150404. https://doi.org/10.1103/PhysRevLett.134.150404.

 doi:10.20944/preprints202602.1143.v1

130. Huang, J.; Qian, X.; Qin, M. Nonstabilizerness entanglement entropy: A measure of hardness in the classical simulation of quantum many-body systems with tensor network states. *Phys. Rev. A* **2025**, *112*, 012425. https://doi.org/10.1103/gxdn-zwrw.
131. Qian, X.; Huang, J.; Qin, M. Augmenting Density Matrix Renormalization Group with Clifford Circuits. *Phys. Rev. Lett.* **2024**, *133*, 190402. https://doi.org/10.1103/PhysRevLett.133.190402.
132. Frau, M.; Tarabunga, P.S.; Collura, M.; Tirrito, E.; Dalmonte, M. Stabilizer disentangling of conformal field theories. *SciPost Phys.* **2025**, *18*, 165. https://doi.org/10.21468/SciPostPhys.18.5.165.
133. Fan, C.; Qian, X.; Zhang, H.C.; Huang, R.Z.; Qin, M.; Xiang, T. Disentangling critical quantum spin chains with Clifford circuits. *Phys. Rev. B* **2025**, *111*, 085121. https://doi.org/10.1103/PhysRevB.111.085121.
134. Huang, J.; Qian, X.; Qin, M. Clifford circuits Augmented Matrix Product States for fermion systems. *arXiv:2501.00413* **2024**.
135. Ding, Y.M.; Wang, Z.; Yan, Z. Evaluating Many-Body Stabilizer Rényi Entropy by Sampling Reduced Pauli Strings: Singularities, Volume Law, and Nonlocal Magic. *PRX Quantum* **2025**, *6*, 030328. https://doi.org/10.1103/pyzr-jmvw.
136. Korbany, D.A.; Gullans, M.J.; Piroli, L. Long-range nonstabilizerness and phases of matter. *arXiv:2502.19504* **2025**.
137. Tarabunga, P.S.; Haug, T. Efficient mutual magic and magic capacity with matrix product states. *arXiv:2504.07230* **2025**.
138. Szombathy, D.; Valli, A.; Moca, C.P.; Farkas, L.; Zaránd, G. Independent stabilizer Rényi entropy and entanglement fluctuations in random unitary circuits. *arXiv:2501.11489* **2025**.
139. Hou, Z.Y.; Cao, C.; Yang, Z.C. Stabilizer Entanglement Enhances Magic Injection. *arXiv:2503.20873* **2025**.
140. Hoshino, M.; Oshikawa, M.; Ashida, Y. Stabilizer Rényi Entropy and Conformal Field Theory. *arXiv:2503.13599* **2025**.
141. Tarabunga, P.S.; Tirrito, E. Magic transition in measurement-only circuits. *arXiv:2407.15939* **2024**.
142. Tirrito, E.; Lumia, L.; Paviglianiti, A.; Lami, G.; Silva, A.; Turkeshi, X.; Collura, M. Magic phase transitions in monitored gaussian fermions. *arXiv:2507.07179* **2025**.
143. Wang, C.; Yang, Z.C.; Zhou, T.; Chen, X. Magic transition in monitored free fermion dynamics. *arXiv:2507.10688* **2025**.
144. Santra, G.C.; Windey, A.; Bandyopadhyay, S.; Legramandi, A.; Hauke, P. Complexity transitions in chaotic quantum systems. *arXiv:2505.09707* **2025**.
145. Haug, T.; Aolita, L.; Kim, M. Probing quantum complexity via universal saturation of stabilizer entropies. *Quantum* **2025**, *9*, 1801. https://doi.org/10.22331/q-2025-07-21-1801.
146. Haug, T.; Piroli, L. Stabilizer entropies and nonstabilizerness monotones. *Quantum* **2023**, *7*, 1092. https://doi.org/10.22331/q-2023-08-28-1092.
147. Haug, T.; Piroli, L. Quantifying nonstabilizerness of matrix product states. *Physical Review B* **2023**, *107*, 035148. https://doi.org/10.1103/physrevb.107.035148.
148. Lami, G.; Collura, M. Nonstabilizerness via Perfect Pauli Sampling of Matrix Product States. *Phys. Rev. Lett.* **2023**, *131*, 180401. https://doi.org/10.1103/PhysRevLett.131.180401.
149. Lami, G.; Collura, M. Unveiling the Stabilizer Group of a Matrix Product State. *Phys. Rev. Lett.* **2024**, *133*, 010602. https://doi.org/10.1103/PhysRevLett.133.010602.
150. Tarabunga, P.S.; Tirrito, E.; Chanda, T.; Dalmonte, M. Many-Body Magic Via Pauli-Markov Chains—From Criticality to Gauge Theories. *PRX Quantum* **2023**, *4*, 040317. https://doi.org/10.1103/PRXQuantum.4.040317.
151. Tarabunga, P.S.; Tirrito, E.; Bañuls, M.C.; Dalmonte, M. Nonstabilizerness via Matrix Product States in the Pauli Basis. *Phys. Rev. Lett.* **2024**, *133*, 010601. https://doi.org/10.1103/PhysRevLett.133.010601.
152. Aditya, S.; Turkeshi, X.; Sierant, P. Growth and spreading of quantum resources under random circuit dynamics. *arXiv:2512.14827* **2025**.

 doi:10.20944/preprints202602.1143.v1

153. Li, H.Z.; Zhang, Y.R.; Zhao, Y.J.; Huang, X.; Zhong, J.X. Slow growth of quantum magic in disorder-free Stark many-body localization. *arXiv:2512.16859* **2026**.
154. Huang, X.; Li, H.Z.; Zhong, J.X. A fast and exact approach for stabilizer Rényi entropy via the XOR-FWHT algorithm. *arXiv:2512.24685* **2026**.